

OMAE2004-51131

**COUPLED NONLINEAR BARGE MOTIONS: PART II: DETERMINISTIC MODELS
STOCHASTIC MODELS AND STABILITY ANALYSIS**

Solomon C. Yim
Ocean engineering Program
Oregon State University
Corvallis, OR 97331, USA

Tongchate Nakhata
Ocean engineering Program
Oregon State University
Corvallis, OR 97331, USA

Erick T. Huang
1100 23rd Avenue
Naval Facilities Engineering
Service Center
Port Hueneme, CA 93043-4370

ABSTRACT

A computationally efficient quasi-two-degree-of-freedom (Q2DOF) stochastic model and a stability analysis of barges in random seas are presented in this paper. Based on the deterministic 2DOF coupled Roll-Heave model with high-degree polynomial approximation of restoring forces and moments developed in Part I, an attempt is made to further reduce the DOF of the model for efficient stochastic stability analysis by decoupling the heave effects on roll motion, resulting in a one-degree-of-freedom (1DOF) roll-only model. Using the Markov assumption, stochastic differential equations governing the evolution of probability densities of roll-heave and roll responses for the two low-DOF models are derived via the Fokker-Planck formulation. Numerical results of roll responses for the 2DOF and 1DOF models, using direct simulation in the time domain and the path integral solution technique in the probability domain, are compared to determine the effects of neglecting the influence of heave on roll motion and assess the relative computational efforts required. It is observed that the 1DOF model is computationally very efficient and the 2DOF model response predictions are quite accurate. However, the nonlinear roll-heave coupling is found to be significant and needs to be directly taken into account rendering the 1DOF roll-only model inadequate for practical use. The 2DOF model is impractical for long-duration real time response computation due to the insurmountable computational effort required. By taking advantage of the observed strong correlation between measured heave and wave elevation in the

experimental results, an accurate and efficient Q2DOF model is developed by expressing the heave response in the 2DOF model as a function of wave elevation, thus reducing the effective DOF to unity. This Q2DOF model is essential as it reduces the computational effort by a factor of 10^{-5} compared to that of the 2DOF model, thus making practical stochastic analysis possible. A stochastic stability analysis of the barge under operational and survival sea states specified by the US Navy is presented using the Q2DOF model based on first passage time formulation.

INTRODUCTION

The stability of ship-to-shore cargo barges under various sea conditions is important to design engineers, especially those of the US Navy. As discussed in Part I, while a barge in general experiences multidirectional sea conditions in the ocean, one of the most critical scenarios leading to capsizing is beam sea. A significant number of researchers have examined the roll stability of ships in beam seas from a stochastic perspective [1-7]. Robert [1, 2] analyzed the roll motion of a ship using the Fokker-Planck (FP) formulation to obtain the probability distribution of the response. Robert *et al* [3] proposed an averaging approximation to reduce the order of the FP equations from two to one to reduce the computational effort. Dahle *et al* [4] developed a simple probabilistic model and computed the probability of capsizing under specified sea states. Lin and Yim [5] modeled the roll motion of a ship by the FP equation and studied the effects of noise on

deterministic regular wave loads. They showed, similar to the deterministic cases demonstrated by Falzarano *et al* [6] and Nayfeh and Sanchez [7], the ship motion to be governed by two diverse dynamical regions – homoclinic and heteroclinic, where the heteroclinic region relates to capsizing. They also examined chaotic response behavior with noise via probability density functions. Kwon *et al* [8] analyzed the roll motion of a ship subjected to an equivalent white noise ocean wave model. Their study focused on the mean upcrossing times for a vessel with nonlinear righting moment and damping. Cai *et al* [9] analyzed the nonlinear roll response of a ship to stationary Gaussian random waves with non-white broadband spectra. The total roll energy was approximated as a Markov process, using a modified version of quasi-conservative averaging. They treated the capsizing of the ship as a first passage problem.

In this paper we begin the study the barge motions under beam sea by first deriving corresponding stochastic models of the deterministic coupled Roll-Heave (2DOF) model developed in Part I and developing a pure Roll (1DOF) in a following section. The path integral solution is employed to numerically obtain the evolutions of barge response probability densities as a solution to the corresponding FP equation of these models. Importance of coupling effects of heave on roll motion is examined by comparing numerical results obtained from the 2DOF and 1DOF models in both time and probability domains. A quasi-2DOF (Q2DOF) model is then developed to take advantage of the observed heave and wave elevation relationship in modeling the roll-heave coupling effects while keeping the number of governing equations to unity. Stability analysis of the barge in terms of reliability against capsizing under various sea states is performed using a first passage time formulation and the quasi-2DOF model.

Governing Equations for Roll-Heave and Roll Models

2DOF Roll-Heave Model -- We start with the deterministic 2DOF model governing the dynamics of fluid-structure interaction behavior of a barge in beam sea derived in Part I. Recall that the model retains the nonlinear coupling effects between roll and heave but removes the tertiary sway effect from equilibrium consideration. The hydrostatic terms are represented efficiently and accurately in the form of high-degree (13th in roll and 12th in heave) polynomials to represent the characteristics of restoring force and moment. Hydrodynamic terms are in a “Morison” type quadratic form.

$$m \ddot{z} + m_{a33} (\dot{z} - \dot{w}) + C_{33L} \dot{z} + C_{33N} z \left| \dot{z} \right| - m(z_g \cos \phi) \phi^2 + mg + R_{33}(z, \phi, \eta, \frac{\partial \eta}{\partial y}) = 0$$

$$I_{44} \ddot{\phi} + I_{a44} (\ddot{\phi} - \frac{\partial \ddot{\eta}}{\partial y}) + C_{44L} (\dot{\phi} - \frac{\partial \dot{\eta}}{\partial y}) + C_{44N} (\phi - \frac{\partial \eta}{\partial y}) \left| \dot{\phi} - \frac{\partial \dot{\eta}}{\partial y} \right| + m(z_g \cos \phi) \dot{\phi} \dot{z} + R_{44}(\phi, z, \eta, \frac{\partial \eta}{\partial y}) - mgz_g \sin \phi = 0 \quad (1)$$

This low DOF, high order polynomial model was developed taking into consideration the strengths of stochastic method to be developed in this study.

1DOF Roll-Only Model – In anticipation of the heavy computational requirement for stochastic analysis of the 2DOF model (see later section), an attempt is made here to further reduce the dimension of the probability domain by possibly employing a 1DOF model. Assuming coupling between roll

and heave is negligible, hence the effects of heave on roll motion can be neglected, the corresponding Roll-only model is derived by neglecting heave-related terms in governing equation for roll in Equation (1)

$$I_{44} \ddot{\phi} + I_{a44} (\ddot{\phi} - \frac{\partial \ddot{\eta}}{\partial y}) + C_{44L} (\dot{\phi} - \frac{\partial \dot{\eta}}{\partial y}) + C_{44N} (\phi - \frac{\partial \eta}{\partial y}) \left| \dot{\phi} - \frac{\partial \dot{\eta}}{\partial y} \right| + R_{44}(\phi, \frac{\partial \eta}{\partial y}) - mgz_g \sin \phi = 0 \quad (2)$$

The physical assumptions of these models are summarized in Part I.

Random Wave Model – As explained in Part I, although the barges considered operate from relatively deep to shallow water, the deep-water condition in general produces higher coupling effects of heave on roll due to larger vertical wave velocity. Therefore, to be conservative, the deep-water condition is employed throughout in this study. For convenience of analysis and simulation of random wave excitation, filtered white noise is used to model random wave surface elevation. The linear filter is defined as

$$\ddot{\eta} + \beta_n \dot{\eta} + (2\pi f_0)^2 \eta = \xi \quad (3)$$

where ξ is Gaussian white noise, which is obtained by using a pseudo random number generator. The transfer function and the spectral density function of the output of the filtered white noise [5] are

$$|H(f)| = \{ [-(2\pi f)^2 + (2\pi f_0)^2]^2 + (2\pi \beta_n)^2 \}^{1/2}$$

$$S_\eta(f) = \{ S_0 / [[-(2\pi f)^2 + (2\pi f_0)^2]^2 + (2\pi \beta_n)^2] \} \quad (4)$$

The coefficients in Equation (4) are set to satisfy the variance and peak period of the Bretschneider spectrum [10] to characterize the random waves, and is expressed as

$$S(\omega) = 0.1687 H_s^2 \frac{\omega_s^4}{\omega^5} e^{-0.675 (\omega_s / \omega)^4} \quad (5)$$

Equation (3) is then reduced to a set of two first-order stochastic differential equations and combined with the equations of motion for the 2DOF and 1DOF models. This stochastic modeling procedure produces, in general, a system of six first-order stochastic differential equations (SDEs) of motion for the 2DOF model and a system of four first-order SDEs for the 1DOF model. Note that for stochastic study, it is important to keep the total DOF of the model low so that the dimension of the probability domain remains low, and the computational efforts manageable. However, the degrees of the polynomial approximations of the stochastic expressions resulting from the high-degree approximating polynomials of the restoring force and moment do not significantly influence the overall computational efforts when joint probability density functions and probability of exceedence are calculated.

Time Domain Predictions

To obtain barge responses in the time domain, the systems of first-order stochastic differential equations for the 2DOF and 1DOF models are solved using standard numerical procedure, with the random waves approximated by linear filtered white noise. A 4th order Runge-Kutta method [11] is employed here

for numerical integration and a Gaussian distributed random number generator is used in the filtered white noise model based on Press *et al* [11].

Probability Domain Predictions

By assuming the stochastic response is a function of only the most recent probability states, a Markov process assumption can be applied. Barge response probability density is numerically derived as a solution to the associated Fokker-Planck equation (FPE) by the path integral solution [12-14]. A general nonlinear stochastic system can be written as

$$\dot{X} = F(X) + G(X)\eta(t) \quad (6)$$

where

$$X = [x_1 \ x_2 \ \dots \ x_N]^T, \ F(X, t) = [F_1 \ F_2 \ \dots \ F_N]^T, \ G(X) = [G_1 \ G_2 \ \dots \ G_N]^T \quad (7)$$

For Equation 7 the associated FPE is

$$\frac{\partial f(X, t)}{\partial t} = Lf(X, t) \quad (8)$$

where the operator

$$L = \frac{1}{2} \frac{\partial^2}{\partial x_\nu \partial x_\mu} Q_{\nu\mu}(X) - \frac{\partial}{\partial x_\nu} K_\nu(X, t); \ \nu, \mu = 1, 2, \dots, N \quad (9)$$

and

$$K_\nu = F_\nu(X); \quad Q_{\nu\mu} = \kappa G_\nu G_\mu \quad (10)$$

With $f(X, t)$ representing the PDF, K_ν 's ($\nu = 1, 2, \dots, N$) are the entries in the drift vector K , and $Q_{\nu\mu}$ are the entries of the $N \times N$ diffusion matrix Q .

The path-integral solution has been developed by Wissel [12] to solve the FPE. It can be represented by a (discrete) Riemann sum

$$f(X_n, t_n) = \lim_{n \rightarrow \infty} \prod_{i=0}^{n-1} (\mu_i dx_i) \exp \left(-\tau \sum_{j=0}^{n-1} L^*(X_{j+1}, X_j, \tau) \right) f(X_{j+1}, X_j, \tau) f(X_0, t_0) \quad (11)$$

where $\mu_i dx_i$ is the (Wiener) measure in the functional space, and L^* is the Lagrangian. A short transition can be obtained analytically using a first order approximation to Equation (11).

With specified drift vector and diffusion tensor for the FPE, the associated short time propagator (Green's function) is given by [14]

$$P_{t,\tau}(X' | X) = (2\pi\tau)^{-\frac{n}{2}} Q^{-\frac{1}{2}} \exp \left\{ -\frac{\tau}{2} [Q_{\nu\lambda}^{(\lambda)} + K_\nu - \frac{x'_\nu - x_\nu}{\tau}] Q_{\nu\mu}^{-1} \right. \\ \left. [Q_{\mu\rho}^{(\rho)} + K_\mu - \frac{x'_\mu - x_\mu}{\tau}] + \tau K_\nu^{(\nu)} + \frac{\tau}{2} Q_{\nu\mu}^{(\nu\mu)} \right\} \quad (12)$$

Using a multi-dimensional histogram representation of the PDF, the path sum expressed in Equation (11) can be implemented numerically. The probability domain at time t is discretized into a finite number of elements represented by function π

$$P(X, t) = \sum_{i=1}^l \pi(x_1 - x_{1i}) \pi(x_2 - x_{2i}) \dots \pi(x_N - x_{Ni}) f(X, t) \quad (13)$$

where

$$\pi(x_n - x_{ni}) = \begin{cases} 1 & \text{for } x_n - \frac{\Delta x_{n(i-1)}}{2} \leq x \leq x_{n(i)} + \frac{\Delta x_{n(i)}}{2} \\ 0 & \text{otherwise} \end{cases} \quad (14)$$

with $n = 1, 2, \dots, N$. The short-time propagator is also discretized into a short-time transition tensor $T_{kl}(\tau)$. Subscripts k and l represent the discretized probability domain at the pre and post state respectively. The short time propagation can be numerically implemented by determining the most probable position in the phase space and the local random response following a Gaussian distribution. The most probable phase position after short-time propagation for each element is deterministically computed by the drift coefficients. The PDF at time $t + \tau$ can be obtained by summing all the probability mass propagated from time t (and normalizing afterward)

$$P_k(t + \tau) = T_{kl}(\tau) P_l(t) \quad (15)$$

where the transition tensor is given by

$$T_{kl}(\tau) = \frac{2^N}{(\Delta x_{kl(i-1)} + \Delta x_{kl(i)}) \dots (\Delta x_{kl(n(j-1)} + \Delta x_{kl(n(j))})} \int_{x_{kl(i)} - \frac{\Delta x_{kl(i-1)}}{2}}^{x_{kl(i)} + \frac{\Delta x_{kl(i)}}{2}} dx_{k1} \dots \int_{x_{kl(n)} - \frac{\Delta x_{kl(n-1)}}{2}}^{x_{kl(n)} + \frac{\Delta x_{kl(n)}}{2}} dx_{kN} \\ \int_{x_{kl(i)} - \frac{\Delta x_{kl(i-1)}}{2}}^{x_{kl(i)} + \frac{\Delta x_{kl(i)}}{2}} dx_{l1} \dots \int_{x_{kl(n)} - \frac{\Delta x_{kl(n-1)}}{2}}^{x_{kl(n)} + \frac{\Delta x_{kl(n)}}{2}} dx_{lN} P_{l,\tau}(X_k | X_l) \quad (16)$$

The PDF at a desired time can be obtained by applying the short time transition in Equation (16) iteratively.

To obtain numerical results, the initial conditions are assumed deterministic, represented by the product of two Dirac delta functions

$$P(X, t_0) = \delta(x_1 - x_{10}) \delta(x_2 - x_{20}) \quad (17)$$

which is represented by a point with area virtually zero in the phase space. For accuracy, the grid size of the discretized probability domain has to be sufficiently small. Moreover, the time step (τ) has to be compatible with the associated grid size. For a given grid size, too small a time step results in no propagation of the probability mass. However, too large a time step is not theoretically appropriate and would lead to inaccurate results. Therefore, the selected time step (τ) in this study is the smallest one that produces propagation of probability mass for a given grid size.

The path integral solution is a first order Euler approximation [12-14], and one possible numerical evaluation based on lattice representation (path sum) [15] can be applied to implement the solution numerically. Using this standard numerical procedure, the evolution of the response density can be computed.

2DOF stochastic model – With the Bretschneider random waves approximated by a linear filtered white noise process and the addition of wave variables into the 2DOF governing equations, the set of six stochastic differential equations can be presented in a system form as

$$\frac{d}{dt} \begin{bmatrix} X_1 \\ X_2 \\ X_3 \\ X_4 \\ \eta_1 \\ \eta_2 \end{bmatrix} = \begin{bmatrix} X_2 \\ \dot{X}_2 \\ X_4 \\ \dot{X}_4 \\ \eta_2 \\ \dot{\eta}_2 \end{bmatrix} + \begin{bmatrix} 0 \\ 0 \\ 0 \\ 0 \\ 0 \\ \xi \end{bmatrix} \quad (18)$$

The corresponding Fokker-Planck equation is given by

$$\begin{aligned} \partial P(X_1, X_2, X_3, X_4, \eta_1, \eta_2, t) = & -\frac{\partial [X_2 P]}{\partial X_1} - \frac{\partial [\dot{X}_2 P]}{\partial X_2} - \frac{\partial [X_4 P]}{\partial X_3} - \frac{\partial [\dot{X}_4 P]}{\partial X_4} \\ & - \frac{\partial [\eta_2 P]}{\partial \eta_1} - \frac{\partial [\dot{\eta}_2]}{\partial \eta_2} + \frac{\kappa}{2} \frac{\partial^2 P}{\partial \eta_2^2} \end{aligned} \quad (19)$$

where

$$\begin{aligned} \dot{X}_2 = & \frac{I_{a44} \frac{\partial \ddot{\eta}}{\partial y} - C_{44i} (X_2 - \frac{\partial \dot{\eta}}{\partial y}) - C_{44v} (X_2 - \frac{\partial \dot{\eta}}{\partial y}) \left| X_2 - \frac{\partial \dot{\eta}}{\partial y} \right| - R_{44} (X_1, \frac{\partial \eta}{\partial y}) + mgz_g \sin(X_1)}{(I_{44} + I_{a44})} \\ \dot{X}_4 = & \frac{m_{a33} \omega^2 \eta_1 - C_{33i} X_4 - C_{33v} X_4 |X_4| + mz_g \cos(X_1) X_2^2 - mg - R_{33} (X_1, X_3, \eta_1, \frac{\partial \eta}{\partial y})}{m + m_{a33}} \end{aligned}$$

$$\dot{\eta}_2 = -\beta_n \eta_2 - (2\pi f_0)^2 \eta_1$$

The corresponding short-time propagator is given by

$$\begin{aligned} G(X'_1, X'_2, X'_3, X'_4, \eta'_1, \eta'_2, X_1, X_2, \eta_1, \eta_2, t; \tau) = & (2\pi\tau)^{-4} \kappa^{-1/2} \exp\left(\frac{-\tau}{2\kappa} (\sigma^2 \eta_2 + \Omega_f^2 \eta_1 + \frac{\eta'_2 - \eta_2}{\tau})^2\right) \\ & \delta(X'_2 - \frac{\eta'_2 - \eta_2}{\tau}) \delta(X'_3 - \frac{X'_1 - X_1}{\tau}) \delta(\eta'_2 - \frac{\eta'_1 - \eta_1}{\tau}) \\ & \delta(X'_4 - \frac{\eta'_2 - \eta_2}{\tau}) \delta(X'_4 - \frac{X'_1 - X_1}{\tau}) \end{aligned} \quad (20)$$

1DOF stochastic model

As before with the Bretschneider random waves approximated by a linear filtered white noise process and the addition of wave variables into the governing equations, the set of four stochastic differential equations for the 1DOF model can be presented in system form as

$$\frac{d}{dt} \begin{bmatrix} X_1 \\ X_2 \\ \eta_1 \\ \eta_2 \end{bmatrix} = \begin{bmatrix} X_2 \\ \dot{X}_2 \\ \eta_2 \\ \dot{\eta}_2 \end{bmatrix} + \begin{bmatrix} 0 \\ 0 \\ 0 \\ \xi \end{bmatrix} \quad (21)$$

$$\partial P(X_1, X_2, \eta_1, \eta_2, t) = -\frac{\partial [X_2 P]}{\partial X_1} - \frac{\partial [\dot{X}_2 P]}{\partial X_2} - \frac{\partial [\eta_2 P]}{\partial \eta_1} - \frac{\partial [\dot{\eta}_2]}{\partial \eta_2} + \frac{\kappa}{2} \frac{\partial^2 P}{\partial \eta_2^2} \quad (22)$$

where the corresponding Fokker-Planck equation is given by

$$\dot{X}_2 = \frac{I_{a44} \frac{\partial \ddot{\eta}}{\partial y} - C_{44i} (X_2 - \frac{\partial \dot{\eta}}{\partial y}) - C_{44v} (X_2 - \frac{\partial \dot{\eta}}{\partial y}) \left| X_2 - \frac{\partial \dot{\eta}}{\partial y} \right| - R_{44} (X_1, \frac{\partial \eta}{\partial y}) + mgz_g \sin(X_1)}{(I_{44} + I_{a44})}$$

and

$$\dot{\eta}_2 = -\beta_n \eta_2 - (2\pi f_0)^2 \eta_1$$

The corresponding short-time propagator is given by

$$G(X'_1, X'_2, \eta'_1, \eta'_2, X_1, X_2, \eta_1, \eta_2, t; \tau) = (2\pi\tau)^{-4} \kappa^{-1/2} \exp\left(\frac{-\tau}{2\kappa} (\sigma^2 \eta_2 + \Omega_f^2 \eta_1 + \frac{\eta'_2 - \eta_2}{\tau})^2\right) \delta(X'_2 - \frac{\eta'_2 - \eta_2}{\tau}) \delta(X'_2 - \frac{X'_1 - X_1}{\tau}) \delta(\eta'_2 - \frac{\eta'_1 - \eta_1}{\tau}) \quad (23)$$

Model Parameters

The model parameters employed in this study were identified in Part I (first numerical column of Table 1) by matching numerical predictions with experimental results in the time domain for six regular wave model test cases (SB26 to SB31). The parameters were validated by comparisons with results from experimental results of a random-wave case.

Coupling Effects of Heave on Roll Barge Motion

Barge roll responses predicted by the 2DOF and 1DOF models using time domain simulation and path-integral solution procedure are examined in this section. Several regular and random waves are used as excitations (see Part I for regular wave generation). Figures 1a and b show barge roll responses to regular waves with $H = 6$ ft and $T = 8$ seconds, and to random wave with $H_s = 4.7$ ft and $T_p = 8.2$ seconds, respectively. For these cases, numerical results indicate good agreement between the 2DOF and the 1DOF models, with the 2DOF model produces slightly larger roll amplitude. However, the differences increase significantly in those cases with larger roll responses, as shown in Fig. 2. Numerical results from the probability domain simulation also indicate the same behavior. Predicted roll response densities under random waves with $H_s = 4.7$ ft and $T_p = 8.2$ seconds, and random waves with $H_s = 5.5$ ft and $T_p = 5.5$ seconds for the 2DOF and 1DOF models after 5 minutes of exposure time in random waves are shown in Figs. 3 and 4, respectively. The corresponding marginal densities of roll motion for both models are presented in Fig. 5. A comparison of the results reveals that the 2DOF model produces greater density at larger roll amplitude at the same exposure time. Additional numerical results also indicate that these differences become more significant for cases with larger roll motion. Based on these observations, the roll motion prediction accuracy of the 1DOF model examined above is deemed unacceptable for practical design, and a more accurate yet computational efficient model needs to be developed.

Computational Efforts of 2DOF and 1DOF Models

The computational effort required for the prediction of stochastic response of the 2DOF model for a short duration, e.g., 10 minute real-time response, using sufficiently fine grid, is on the order of two to three months using a well equipped

state-of-the-art Sun Workstation. For the corresponding 1DOF model, the same real time response duration can be solved within a few minutes (approximately 10^{-5} times the computational effort of the 2DOF system). For longer runs for low sea state responses analysis (e.g., 10 hours of real time response, as discussed in the following sections), the computational time required for the 2DOF model is on the order of 10 years. This is obviously unacceptable, thus a low DOF yet accurate approximate model, which retains the heave-roll coupling effects, needs to be developed.

Efficient Quasi-2DOF Model

The governing equations of motion of the 2DOF model show that the coupling effects of heave on roll are represented in two distinctive mechanisms. First, the relative heave motion to wave elevation impact the hydrostatic roll righting moment. Second, the heave velocity creates inertia moment caused by eccentricity of the roll center and KG. These relationships are explored in detail in this section to develop a computationally efficient yet accurate approximate model including the heave-roll coupling effects.

Typical time histories of barge heave responses to regular and random waves based on experimental results are shown in Fig. 6. It is observed that the relative motions between heave and wave elevation are small. Based on this assumption, a quasi-2DOF model is developed here with the heave motion approximated by wave elevation is derived. In this case, the hydrostatic roll restoring moment is not affected by heave and the coupling effects of heave and roll are presented only via the inertia moment caused by eccentricity of roll center and KG.

The quasi-2DOF model can be developed by approximating the heave velocity by the vertical wave velocity in the equation of motion of the 1DOF model that represents heave-induced inertia moment due to eccentricity of roll center and KG. The resulting equation of motion of this approximate model is

$$I_{44} \ddot{\phi} + I_{a44} \left(\ddot{\phi} - \frac{\partial \ddot{\eta}}{\partial y} \right) + C_{44L} \left(\dot{\phi} - \frac{\partial \dot{\eta}}{\partial y} \right) + C_{44V} \left(\phi - \frac{\partial \eta}{\partial y} \right) \left| \dot{\phi} - \frac{\partial \dot{\eta}}{\partial y} \right| + m(z_g \cos \phi) \dot{\phi} \dot{w} + R_{44}(\phi, z, \eta, \frac{\partial \eta}{\partial y}) - mgz_g \sin \phi = 0 \quad (24)$$

The advantage of the Q2DOF model is that it retains a majority of the coupling effects of heave effect on roll motion while keeping the DOF of the model at unity. While the path-integral solution of the FPE for the 2DOF model requires 10^5 times the computational effort of that of the corresponding 1DOF model, the Q2DOF model solution takes only about 1.5 times of that of the 1DOF model.

Time and probability domain simulations of the Q2DOF model using regular and random waves as excitation are performed to assess its response prediction accuracy (Figs. 7 and 8, respectively). These figures indicate a significant improvement in the predictive capability of the Q2DOF model over the 1DOF model, and the predictive results are very close to those obtained from the 2DOF model. Based on these and additional numerical results (not presented here due to space limitation), the Q2DOF model is deemed sufficiently accurate for detail stability analysis of barges.

Stability Analysis

Stability of the roll motion of a barge over a range of sea states under beam sea is analyzed here using the first-passage-time formulation. As the barge rolls in random seas, the net roll response density propagates with time and eventually exits the safe domain. In this study, net roll is defined as the difference between roll angle and wave slope. Hydrostatic roll restoring moment indicates a zero value once net roll exceeds 58 degrees for the ship-to-shore cargo barge as shown in Fig. 9. Reliability against capsizing of the barge is defined as the cumulative net roll response density, which lies within the safe domain (in this case ± 58 degrees). At a given time t , the reliability is given by

$$Wo(t) = \int_{\tilde{\phi}=-58}^{\tilde{\phi}=58} P(\tilde{\phi}, \dot{\tilde{\phi}}) d\tilde{\phi} \quad (25)$$

Using the US Navy specification, the range of sea states 1 through 9 are represented by their average significant wave height, H_s , and spectral peak periods, T_p , as shown in Table 1. In this study, stochastic excitations according to each sea state are applied to the Q2DOF model. The evolution of the net roll response density and reliability for these sea states are computed. Because similarities of responses among various sea states, for succinctness of presentation, only representative results (sea states 1, 4, 7 and 9) are shown in Figs. 10 through 13. The numerical results indicate negligible likelihood of capsizing for barges operating under sea state 1 (and similar for sea state 2) in 10 hours of exposure time due to low amplitude in the wave excitation (Fig. 10). While the peak period of the wave excitations may be near heave resonance, the energy dissipation (or damping) in heave is sufficiently large to prevent large-amplitude resonance. This observation was verified via direct simulation of motions response from the more accurate 3DOF and 2DOF models.

It is observed that the behavior of the barge roll motion is similar for sea states 3 through 6 (see Fig. 11 for sea state 4 results), and it takes approximately 1 to 3 hours for barges operating in these sea states to attain 1% probability of capsizing. Figs. 12 and 13 show the probability density and reliability of the barge for sea states 7 and 9, respectively, for specific durations of exposure. These results indicate significantly larger probability of capsizing in a short period of time.

The probability information of the barge response for sea states 3 through 9 is presented in Fig. 14 in a summary form in terms of time to reach 1, 2, 5 and 10 percent probability of capsizing. Note that while the expected exposure time declines gradually with increasing sea states from 3 to 6, there is a sharp drop between sea states 6 and 7. The rate of decline in expected exposure time from sea states 7 through 9 is also significantly higher than those from sea states 3 through 6. The probability of capsizing of the barge in sea states 1 and 2 over a 10-hour exposure is significantly less than 1%, thus results are not shown in Fig. 14. It should be pointed out here that while the range of responses of the experimental results employed in Part I to validate the numerical models only reached ± 15 degrees, we rely on the numerical models to extrapolate to results into the highly nonlinear capsizing region here. This is unfortunately necessary as there was no data available near the capsizing region due to experimental limitations.

Table 1 Average significant wave height and spectral peak period of sea states 1 through 9

Sea State	Significant wave height H_s (ft)	Spectral peak period T_p (second)
1	0.5	2.4
2	2.0	4.6
3	4.0	6.0
4	6.5	7.5
5	10.0	8.9
6	16.0	10.8
7	30.0	13.6
8	50.0	17.0
9	100.0	22.4

Concluding Remarks

A stochastic analysis of the Roll-Heave (2DOF) and Roll-only (1DOF) barge motion models is presented here. With the Markov process assumption, associated Fokker-Planck equations of the deterministic models presented in [8] are derived and the corresponding path integral solutions are used to obtain barge response probability densities numerically.

To determine the importance of the heave-on-roll coupling effects, a comparison of the predicted roll motions derived from the Roll-Heave and the Roll-only models using time and probability domain simulations is performed. Results show that the 2DOF model predicts similar, but slightly larger-amplitude roll motion than the 1DOF model under low level of wave excitations. However, the difference becomes more significant under higher sea states where roll motion is larger. The prediction capability of the 1DOF model is deemed inadequate for practical application. However, the 2DOF stochastic model requires excessive computational time for practical analysis and design.

A close examination of the governing equations of motion reveal that heave affects roll motion via the hydrostatic roll restoring moment and the initiating inertia moment due to the eccentricity of roll center and KG. Experimental results showed that, for the barges examined, the relative motion between heave and wave elevation is negligibly small. Thus, the heave impact on the hydrostatic righting moment is negligible.

To address the need for an accurate yet efficient predictive model for reliability analysis, a quasi-2DOF model is developed by expressing heave in terms of wave elevation to preserve the coupling effects of heave on roll motion in the 2DOF model. Specifically, heave velocity is approximated by vertical wave velocity to approximate inertia moment caused by coupling between heave velocity and the eccentricity of roll center and KG. Time and probability domain simulations indicate that the quasi-2DOF model retain the predictive capability of the 2DOF model and yet requires only 10^{-5} times the computational effort.

Stability analysis of the barge under the entire range of sea states (1 through 9) considered by the US Navy is performed using a first-passage-time formulation with the quasi-2DOF model. The response density evolutions are obtained via the path-integral solution to the associated Fokker-Planck equation.

Exposure times that create capsizing probability of 1, 2, 5 and 10 percent are presented for selected sea states. Results indicate that the reliability of barge is significantly reduced when operating under sea states 7 or higher. Numerical results show that for sea states 1 and 2, the probability of capsizing in 10 hours exposure is significantly less than 1%. It takes approximately 1 to 5 hours for a barge operating in sea state 3 through 6 to have 1 to 10 percent overturning probability.

ACKNOWLEDGMENTS

The authors wish to thank the reviewers for their valuable comments and suggestions. Financial support from the United State Office of Naval Research Grant No. N00014-92-1221 is gratefully acknowledged. The authors also wish to acknowledge the Office of Naval Research Seabased Logistics Program under, Dr. P. Abraham, Code 362, for support of investigation of the assessment of barge stability.

REFERENCES

- [1] Roberts, J.B. 1982a. A Stochastic Theory for Nonlinear Ship Rolling in Irregular Seas. *Journal of Ship Research*, 26(4), 229-245.
- [2] Roberts, J.B. 1982b. Effect of Parametric Excitation on Ship Rolling Motion in Random Waves. *Journal of Ship Research*, 26(4), 246-253.
- [3] Robert, J.B., Dunne J.F., and Debonos A. 1994. Stochastic Estimation Methods for Non-Linear Ship Roll Motion. *Probabilistic Engineering Mechanics* 9, 83-93.
- [4] Dahle, E.A., Myhaug, D. and Dahl, S.J. 1988. Probability of Capsizing in Steep and High Waves from the Side in Open Sea and Coastal Waters. *Ocean Engineering*, 15(2), 139-151.
- [5] Lin, H. and Yim, S.C.S. 1995. Chaotic Roll Motion and Capsizing of Ships Under Periodic Excitation with Random Noise. *Applied Ocean Research*, 17(3), 185-204.
- [6] Falzarano, J.M., Shaw, S.W., and Troesch, A.W. 1992. Application of Global Methods for Analyzing Dynamical Systems to Ship Rolling Motion and Capsizing. *International Journal of Bifurcation and Chaos in Applied Sciences and Engineering*, 2(1), 101-116.
- [7] Nayfeh, A.H., and Sanchez, N.E. 1990. Stability and Complicated Rolling Responses of Ships in Regular Beam Sea. *International Shipbuilding Congress*, 37(412), 331-352.
- [8] Kwon, S.H., Kim, D.W. and McGregor, R.C. 1993. A Stochastic Roll Response Analysis of Ships in Irregular Waves. *International Journal of Offshore and Polar Engineering*, 3(1), 32-34.
- [9] Cai, G.Q., Yu, S.J. and Lin, Y.K. 1994. Ship Rolling in Random Sea. *Stochastic Dynamics and Reliability of Nonlinear Ocean Systems*, ASME DE-Vol. 77, 81-88.
- [10] Chakrabarti, S.K. 1994. Hydrodynamics of Offshore Structures, *Computational Mechanics Publications*, Southampton Boston.
- [11] Press W.H., Flannery, B.P., Teukolsky, S.A. and Vetterling, W.T. 1986. *Numerical Recipes*, Cambridge University Press.
- [12] Naess, A., and Johnsen, J.M., Statistics of Nonlinear Dynamic Systems by path integrations. *Nonlinear Stochastic Mechanics*: 401-409.
- [13] Naess, A. and Johnsen, J.M., 1993. Response Statistic of Nonlinear, Compliant Offshore Structures by the Path Integral

Solution Method. *Probabilistic Engineering Mechanics*, 8, 91-106.

[14] Wissel, C. 1979. Manifolds of Equivalent Path Integral Solutions of the Fokker-Planck Equation. *Zeitschrift für physik B*, 35, 185-191.

[15] Wehner, M.F., and Wolfer, W.G. 1983. Numerical Evaluation of Path-Integral Solutions to Fokker-Planck Equations, *Physical Review A*, 27, 2663-2670.

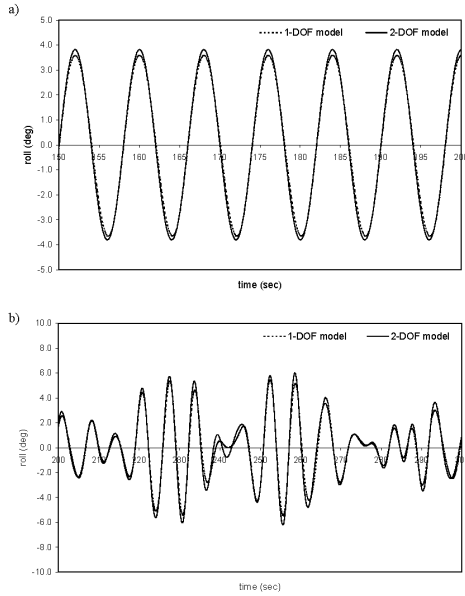


Figure 1 Comparison of barge roll response time histories predicted by 2DOF and 1DOF models under (a) regular waves with $H = 6$ ft and $T = 8$ seconds, and (b) random waves with $H_r = 4.7$ ft and $T_p = 8.2$ seconds.

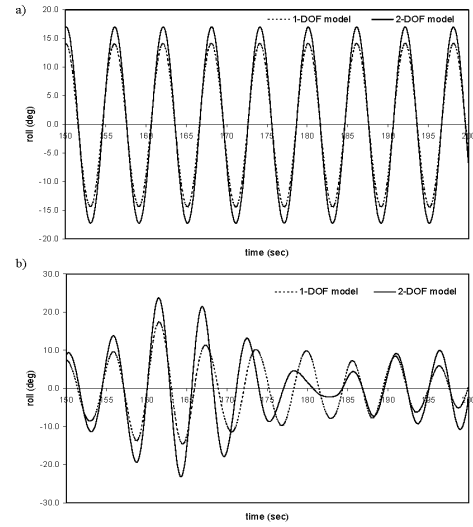


Figure 2 Comparison of barge roll response time histories predicted by 2DOF and 1DOF models under (a) regular waves with $H = 6.5$ ft and $T = 6$ seconds, and (b) random waves with $H_r = 5.5$ ft and $T_p = 6.0$ seconds.

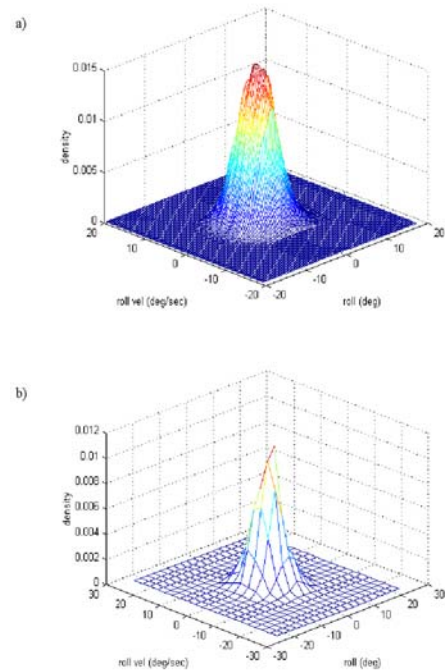


Figure 3 (a) 1DOF model, and (b) 2DOF model path integral solution prediction of probability density of roll response under random waves with $H_r = 4.7$ ft and $T_p = 8.2$ seconds at time $t = 5$ minutes.

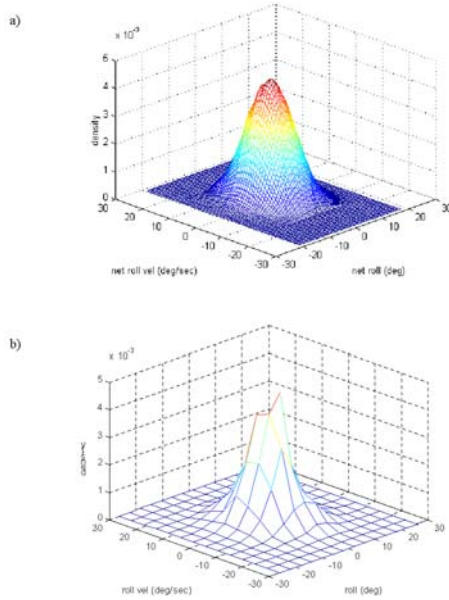


Figure 4 (a) 1DOF model, and (b) 2DOF model path integral solution prediction of probability density of roll response under random waves with $H_s = 5.5$ ft and $T_p = 5.5$ seconds at time $t = 5$ minutes.

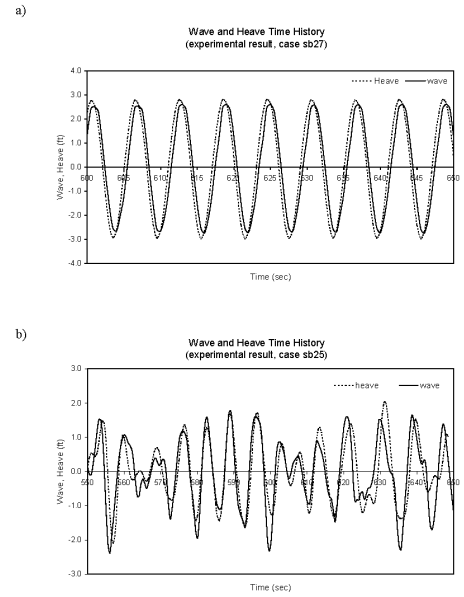


Figure 6 Comparison of measured experimental heave and wave time histories under (a) regular wave with $H = 6$ ft and $T = 6$ seconds, and (b) random wave with $H_s = 4.7$ ft and $T_p = 8.2$ seconds.

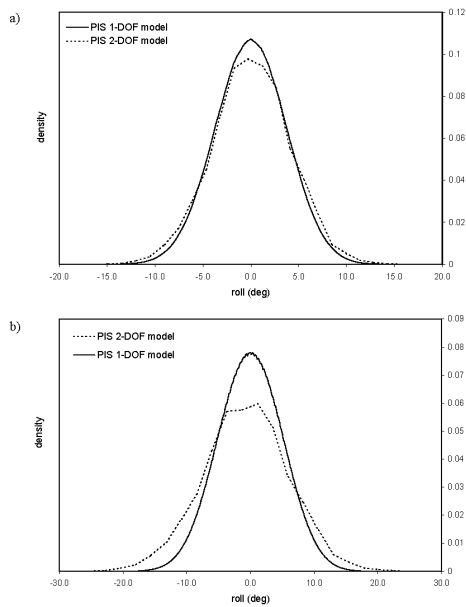


Figure 5 Comparison of roll response marginal probability density between numerical predictions of 2DOF and 1DOF models at time $t = 5$ minutes under random wave with (a) $H_s = 4.7$ ft and $T_p = 8.2$ seconds, and (b) $H_s = 5.5$ ft and $T_p = 5.5$ seconds.

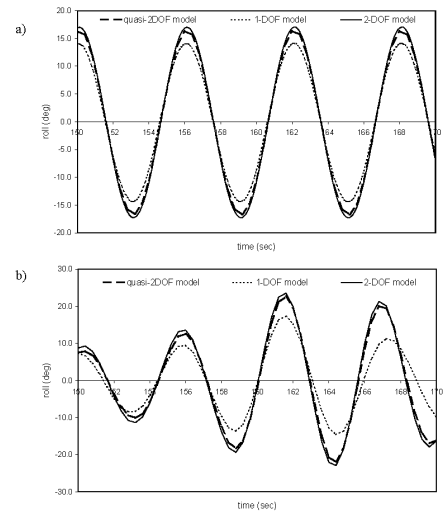


Figure 7 Comparison of predicted barge roll response time histories predicted by 2DOF, 1DOF, and quasi-2DOF models, (a) regular waves with $H = 6.5$ ft and $T = 6$ seconds, and (b) random waves with $H_s = 5.5$ ft and $T_p = 6.0$ seconds.

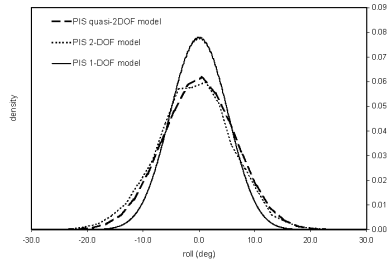


Figure 8 Comparison of roll response marginal density at 5 minutes predicted by 2DOF, 1 DOF, and quasi-2DOF models under random wave excitation with $H_s = 5.5$ ft and $T_p = 5.5$ second.

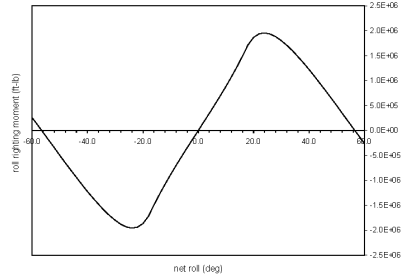


Figure 9 Analytical roll righting moment of barge considered.

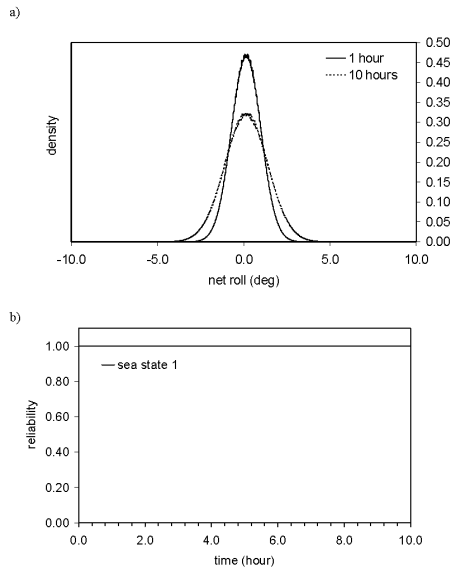


Figure 10 (a) Probability density, and (b) reliability against capsizing of barge roll response to sea state 1 random waves.

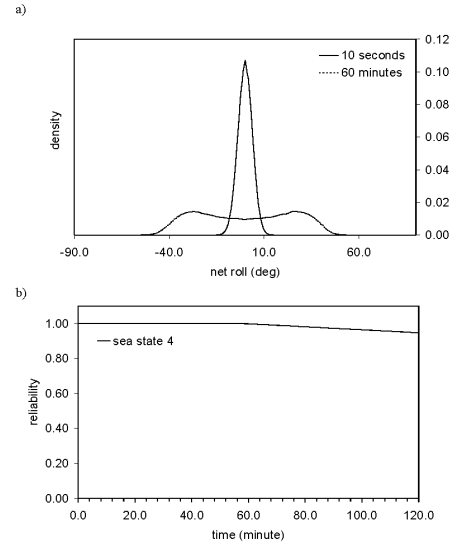


Figure 11 (a) Probability density, and (b) reliability against capsizing of barge roll response to sea state 4 random waves.

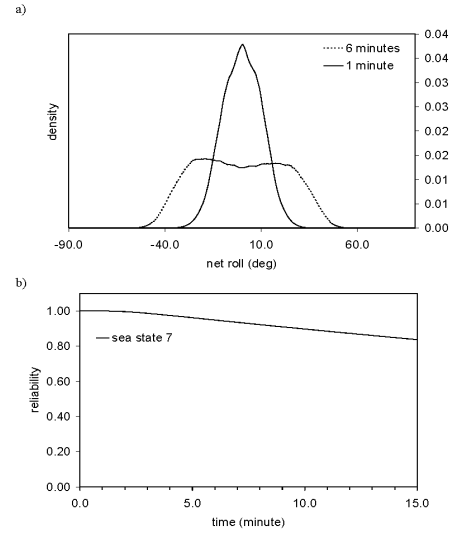


Figure 12 (a) Probability density, and (b) reliability against capsizing of barge roll response to sea state 7 random waves.

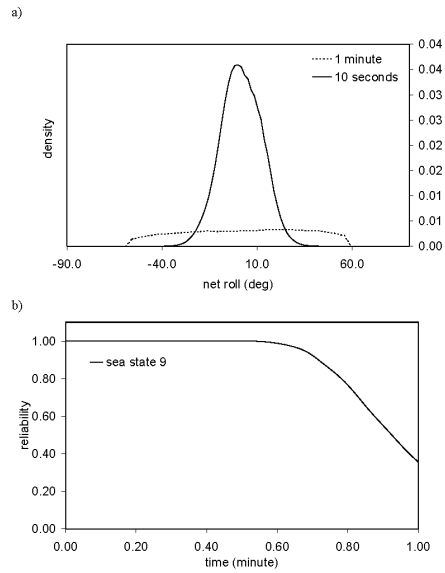


Figure 13 (a) Probability density, and (b) reliability against capsizing of barge roll response to sea state 9 random waves.

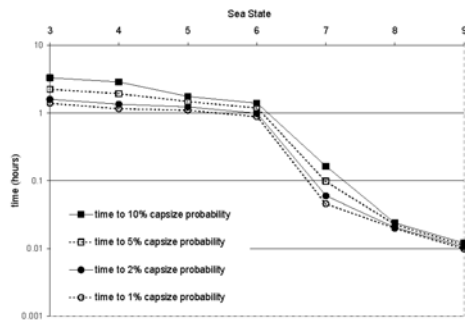


Figure 14 Mean time to reach specified capsizing probabilities for a barge operating in sea states 3 through 9 obtained using quasi-2DOF model.